

# ACE-Merging: Data-Free Model Merging with Adaptive Covariance Estimation

Bo Xu<sup>1</sup> Haotian Wu<sup>1</sup> Hehai Lin<sup>1</sup> Weiquan Huang<sup>1</sup> Beier Zhu<sup>2</sup> Yao Shu<sup>1</sup> Chengwei Qin<sup>1</sup>

<sup>1</sup>The Hong Kong University of Science and Technology (Guangzhou)

<sup>2</sup>University of Science and Technology of China

## Abstract

*Model merging aims to combine multiple task-specific expert models into a single model while preserving generalization across diverse tasks. However, interference among experts, especially when they are trained on different objectives, often leads to significant performance degradation. Despite recent progress, resolving this interference without data access, retraining, or architectural modification remains a fundamental challenge. This paper provides a theoretical analysis demonstrating that the input covariance of each task, which is a key factor for optimal merging, can be implicitly estimated from the parameter differences of its fine-tuned model, even in a fully data-free setting. Building on this insight, we introduce ACE-Merging, an Adaptive Covariance Estimation framework that effectively mitigates inter-task interference. Our approach features a principled, closed-form solution that contrasts with prior iterative or heuristic methods. Extensive experiments on both vision and language benchmarks demonstrate that ACE-Merging sets a new state-of-the-art among data-free methods. It consistently outperforms existing baselines; for example, ACE-Merging achieves an average absolute improvement of 4% over the previous methods across seven tasks on GPT-2. Owing to its efficient closed-form formulation, ACE-Merging delivers superior performance with a modest computational cost, providing a practical and theoretically grounded solution for model merging.*

## 1. Introduction

Driven by advanced architectures like the Transformer [1], the pre-training and fine-tuning paradigm [2] has led to a proliferation of highly specialized expert models. Consolidating the knowledge from these disparate experts is a critical need, yet traditional multi-task training [3] from scratch is often prohibitively expensive or simply infeasible, as organizations frequently release only model weights without the corresponding training data. Recently, *model merging* [4, 5] has emerged as a promising solution, enabling the integration of multiple expert models into a single uni-

fied multi-task model without the need for costly retraining on multi-task datasets. By directly operating on the weights of fine-tuned experts, model merging provides an efficient and data-free alternative for consolidating knowledge across tasks.

Despite its practical appeal, model merging is fundamentally challenged by *inter-task interference*. Existing efforts to mitigate this issue can be grouped into three categories. *Data-dependent* methods [6–8] leverage input statistics to guide the merge, but their reliance on original task data is often impractical due to privacy and accessibility constraints. *Test-time adaptive* methods [9, 10] adjust models during inference, sacrificing the “merge-once, deploy-anywhere” efficiency and introducing substantial computational overhead. This leaves *data-free merging* as the most general and appealing solution: by operating solely on model parameters, it offers maximum flexibility and efficiency. However, this paradigm is fundamentally constrained, as it aims to solve an optimization problem without its most critical input: the statistical structure of task data. Consequently, approaches ranging from the foundational Task Arithmetic [4] to recent sophisticated variants [11–14] remain parameter-space heuristics, addressing only the *symptoms* of interference rather than its *root cause* in the mismatched data distributions.

In this work, we revisit this long-standing challenge from a theoretical perspective. We show that, under a mild linear approximation, the input covariance of each task is implicitly encoded in the parameter changes of its fine-tuned model, providing a previously overlooked bridge between data-level structure and parameter-space behavior. This observation motivates a new formulation of data-free model merging that explicitly accounts for inter-task covariance, enabling principled fusion without requiring any access to task data. This formulation admits to an analytical closed-form solution, which we instantiate as ACE-Merging. To ensure robustness across diverse tasks and model architectures, ACE-Merging includes two key components: (1) an adaptive regularization scheme that accounts for task heterogeneity, and (2) a spectral refinement step that corrects inherent biases in the merging process. Therefore,

ACE-Merging provides a principled and efficient solution that achieves strong performance while maintaining computational efficiency in the data-free setting. Our main contributions are summarized as follows:

- **Foundational theory.** We establish a formal relationship between the parameter changes induced by fine-tuning and the task’s input covariance matrix, providing a principled basis for purely data-free model merging.
- **Unified explanatory framework.** We show that some prior methods, from simple averaging to complex heuristics, can be recast as implicit, often coarse, estimators of the input covariance, which clarifies their disparate empirical behavior.
- **Comprehensive state-of-the-art performance.** Extensive experiments on both language and vision benchmarks demonstrate that ACE-Merging consistently achieves state-of-the-art performance among data-free methods, improving average accuracy by **4%** on GPT-2 across seven tasks and by **5%** on RoBERTa-base, while maintaining competitive efficiency. On several vision benchmarks, ACE-Merging further surpasses data-dependent and test-time adaptation baselines, highlighting its strong generalization and practical scalability.

## 2. Related work

### 2.1. Data-dependent model merging

Data-dependent model merging formulates the fusion as an optimization problem that relies on input-level statistics. Representative approaches exploit feature covariances or Fisher information to weight parameters during aggregation [6–8, 15]. Although effective, their dependence on task data for estimating importance weights limits their applicability in fully data-free settings.

### 2.2. Test-time adaptive model merging

Test-time adaptive methods perform dynamic fusion during inference rather than constructing a single static model. They adjust merging coefficients or lightweight modules on the fly according to the current input or task context [9, 10, 13, 16, 17]. Such approaches often minimize prediction uncertainty or employ routing mechanisms to specialize the merged model for unseen data. While these strategies can yield higher task-specific performance, they introduce additional inference overhead or rely on access to representative test data, limiting their practicality for static deployment.

### 2.3. Data-free model merging

In practical scenarios, access to task data is often limited due to privacy or scalability constraints, making data-free model merging the most general and desirable solution. However, the absence of data also removes the sta-

tistical signals that reveal task relationships, forcing methods to rely on parameter-space heuristics to approximate the underlying data geometry. Early data-free methods rely on mitigate interference through heuristic operations such as sign alignment or parameter pruning [11, 14, 18]. While efficient, these Euclidean-space operations fail to capture deeper structural misalignments between models. More recent work seeks a superior basis for merging, primarily through SVD-based decompositions that isolate shared and task-specific subspaces [19–22]. Concurrently, optimization-inspired methods like WUDI-Merging [23] derive analytical solutions but often rely on iterative gradient descent for their implementation, sacrificing the stability of a true closed-form solution. In summary, data-free merging still lacks a unified and efficient closed-form formulation that captures inter-task structure. ACE-Merging fulfills this need through covariance estimation and spectrally adaptive fusion, achieving superior stability and efficiency over SVD- and gradient-based methods.

## 3. Background and motivation

In this section, we formalize the data-free model merging problem and revisit the optimal objective under a linear assumption, which forms the theoretical basis of our method.

### 3.1. Preliminary of model merging

**Notation.** Let  $\mathcal{M}_0$  denote a pretrained model with layer weights  $\{W_0^l\}_{l \in [L]}$ ,<sup>1</sup> where  $l$  indexes one of the  $L$  layers. Fine-tuning  $\mathcal{M}_0$  on a downstream task  $t$  yields a specialized model with weights  $W_t$ . Following Task Arithmetic [4], we define the *task vector* as the weight displacement  $\Delta W_t = W_t - W_0$ , which captures the task-specific parameter update relative to the pretrained model.

**Model merging objective.** Given  $T$  fine-tuned expert models  $\{\mathcal{M}_t\}_{t \in [T]}$  with parameters  $\{W_t\}_{t \in [T]}$ , our goal is to obtain a unified merged model  $\mathcal{M}$  with parameters  $\bar{W}$  that best preserves the behaviors of all experts across their respective datasets  $\{\mathcal{D}_t\}$ . Formally, we minimize the expected output discrepancy between the merged model and each expert:

$$\min_{\bar{W}} \sum_{t \in [T]} \mathbb{E}_{x \sim \mathcal{D}_t} \|f(\bar{W}, x) - f(W_t, x)\|_2^2. \quad (1)$$

Here,  $f(W, x)$  denotes the layer-wise transformation performed with parameters  $W$  on input feature  $x$ .

### 3.2. Optimal linear merging

To derive a closed-form solution, we linearize the forward mapping as  $f(W, x) \approx Wx$ , a widely adopted approxima-

<sup>1</sup>As our algorithm is applied independently to each layer, we omit the layer index  $l$  in subsequent derivations for clarity.

tion supported by empirical studies [24]. Under this assumption, Eq. (1) reduces to a tractable quadratic form:

$$\mathcal{L}(\bar{W}) = \sum_{t \in [T]} \text{Tr} [(\bar{W} - W_t) \Sigma_t (\bar{W} - W_t)^\top], \quad (2)$$

where  $\Sigma_t = \mathbb{E}_{x \sim \mathcal{D}_t} [xx^\top]$  denotes the input covariance of task  $t$ . Minimizing Eq. (2) with respect to  $\bar{W}$  yields the closed-form solution:

$$\bar{W} = \left( \sum_{t \in [T]} W_t \Sigma_t \right) \left( \sum_{t \in [T]} \Sigma_t \right)^{-1}. \quad (3)$$

This expression exposes covariance as the key factor underlying different merging strategies, motivating a unified reinterpretation of prior methods.

### 3.3. Revisiting baselines through covariance

In this section, we use Eq. (3) to analyze two representative data-free merging methods: Weight-averaging [5] and WUDI-Merging [23].

**Weight averaging.** The simplest baseline assumes uniform and isotropic task covariances, i.e.,  $\hat{\Sigma}_t = kI$  for some constant  $k > 0$ . Substituting this assumption into Eq. (3) yields  $\bar{W} = \frac{1}{T} \sum_{t=1}^T W_t$ , indicating that arithmetic averaging is only optimal under the restrictive condition that all task data distributions share identical statistics.

**Task-specific covariance from task vectors.** Beyond the uniform assumption, a more expressive approach is to estimate the task-specific covariance directly from the task vector  $\Delta W_t$ . A simple data-free proxy for the input second-moment matrix is the outer product of the task vector with itself:  $\hat{\Sigma}_t \propto (\Delta W_t)^\top \Delta W_t$ . Interestingly, the recent WUDI-Merging method, though derived from a different objective and optimized via gradient descent, can be interpreted within our framework as implicitly using a norm-weighted version of this proxy:  $\hat{\Sigma}_t \propto \|\Delta W_t\|_F^{-2} (\Delta W_t)^\top \Delta W_t$ . This perspective suggests that the success of WUDI-Merging arises from employing a more informative, task-specific covariance proxy. However, its reliance on iterative optimization introduces computational overhead and sensitivity to hyperparameters, which further motivates the development of our principled, closed-form estimator presented in the next section.

## 4. Methodology

### 4.1. Estimating input covariance without data

We first establish the theoretical connection between input covariance and fine-tuning updates.

**Theorem 1.** *The input covariance of task  $t$  is proportional to the covariance of its weight displacements:*

$$\Sigma_t \propto \text{Cov}_{\mathcal{D}_t} [\Delta W_t]. \quad (4)$$

*Proof sketch.* We view fine-tuning as a gradient-based transition from the pretrained weights  $W_0$  to the task-specific weights  $W_t$ :

$$\Delta W_t = -\eta \sum_{i=1}^{N_t} \nabla_W \mathcal{L}_t(x_i, W_t^{(i-1)}),$$

where  $\eta$  is the learning rate and  $\mathcal{L}_t$  is the task-specific loss. Since fine-tuning updates are typically small in magnitude [25], the gradients can be linearized around the initialization  $W_0$ , which simplifies the expression to:

$$\Delta W_t \approx -2\eta N_t \mathbb{E}_{(x,y) \sim \mathcal{D}_t} [(W_0 x - y)x^\top].$$

The stated proportionality follows from this approximation. A complete derivation is provided in Appendix A.  $\square$

Eq. (4) is powerful but involves expectations over  $\mathcal{D}_t$ , which are unavailable in data-free settings. To obtain a practical estimator, we treat the rows of  $\Delta W_t$  as independent samples and compute the empirical covariance:

$$\hat{\Sigma}_t \propto (\Delta W_t - \mathbf{1}\mu_t^\top)^\top (\Delta W_t - \mathbf{1}\mu_t^\top), \quad (5)$$

where  $\mu_t = \frac{1}{d_{\text{in}}} \mathbf{1}^\top \Delta W_t$  is the column-wise mean. The proportionality constant only affects scale and thus cancels out in the final solution.

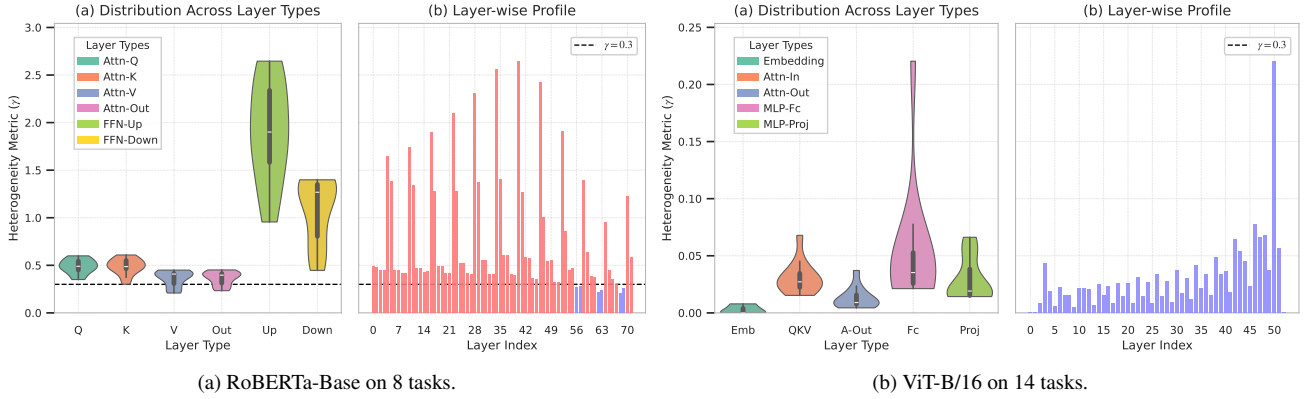
However, directly using this empirical estimator introduces several challenges, including scale imbalance, covariance degeneracy, and instability in heterogeneous task settings. To address these issues, we propose ACE-Merging, which comprises three key components: (1) an adaptive covariance normalization scheme that balances task energy scales and stabilizes inversion; (2) a robust covariance estimator with a collective structural prior; and (3) an optional spectral refinement step that corrects structural imbalances in highly diverse task sets. The following sections detail each component in turn.

### 4.2. Adaptive covariance normalization

A central challenge in model merging lies in the large heterogeneity of energy scales across tasks. When computing the aggregated covariance  $\sum_t \hat{\Sigma}_t$ , high-energy tasks tend to dominate the sum, biasing the merged model toward their representations while suppressing the contributions of low-energy tasks.

To mitigate this imbalance, we introduce an adaptive regularization scheme. Instead of adjusting the regularization coefficient  $\epsilon$ , we normalize each covariance matrix before

Figure 1. Comparison of inter-task heterogeneity ( $\gamma$ ) across architectures. ViT-B/16 shows relatively uniform scaling ( $\gamma < 0.25$ ), while RoBERTa-Base exhibits much stronger variance ( $\gamma > 0.3$ ) across layers. This cross-architecture contrast motivates our adaptive scaling mechanism.



aggregation to equalize task scales. The decision to normalize is guided by a heterogeneity metric  $\gamma$ , defined as:

$$\gamma = \frac{\text{Var}_t [\log \|\Delta W_t\|_F^2]}{(\mathbb{E}_t [\log \|\Delta W_t\|_F^2])^2}. \quad (6)$$

A high  $\gamma$  indicates significant scale divergence, triggering our normalization policy. This heterogeneity varies substantially across architectures (Figure 1), underscoring the need for an adaptive approach.

When strong task heterogeneity is detected ( $\gamma > \tau$ ), each covariance matrix is first normalized by its trace to balance energy scales:

$$\hat{\Sigma}_{t,\text{scaled}} = \frac{\hat{\Sigma}_t}{\text{Tr}(\hat{\Sigma}_t)}. \quad (7)$$

We then apply Tikhonov regularization using an energy-adjusted coefficient to ensure stable inversion:

$$\hat{\Sigma}_{t,\text{reg}} = \hat{\Sigma}_{t,\text{scaled}} + \frac{\epsilon}{\text{Tr}(\hat{\Sigma}_t)} I. \quad (8)$$

For homogeneous task sets ( $\gamma \leq \tau$ ), both steps are skipped, and  $\hat{\Sigma}_t$  is used directly. This adaptive scaling prevents high-energy tasks from dominating the merged covariance while maintaining numerical stability.

### 4.3. Collective structural prior

While the adaptive regularization strategy in Section 4.2 effectively balances task contributions and stabilizes covariance inversion, it still treats all feature dimensions uniformly. The fundamental limitation of this approach lies in its *isotropic* nature, which penalizes every direction equally and ignores the underlying geometry of the input space. In essence, although the  $\epsilon I$  term ensures numerical stability, it remains a structure-blind safeguard rather than an informative prior.

To overcome this limitation, we introduce a data-driven *anisotropic* regularizer that captures the collective feature geometry across tasks. We define the *Collective Structural Prior (CSP)*, denoted  $\mathbf{C}_{\text{agg}}$ , constructed from column-wise statistics of the aggregated task covariances:

$$\mathbf{C}_{\text{agg}} = \mathbf{1} \left( \frac{1}{d_{\text{in}}} \mathbf{1}^\top \sum_{t \in [T]} \hat{\Sigma}_{t,\text{scaled}} \right). \quad (9)$$

where  $\mathbf{1} \in \mathbb{R}^{d_{\text{in}}}$  is the all-ones vector that broadcasts the mean column energy across rows. This yields a low-rank, consensus-driven correction that selectively amplifies dimensions of shared importance. The final close-form solution is:

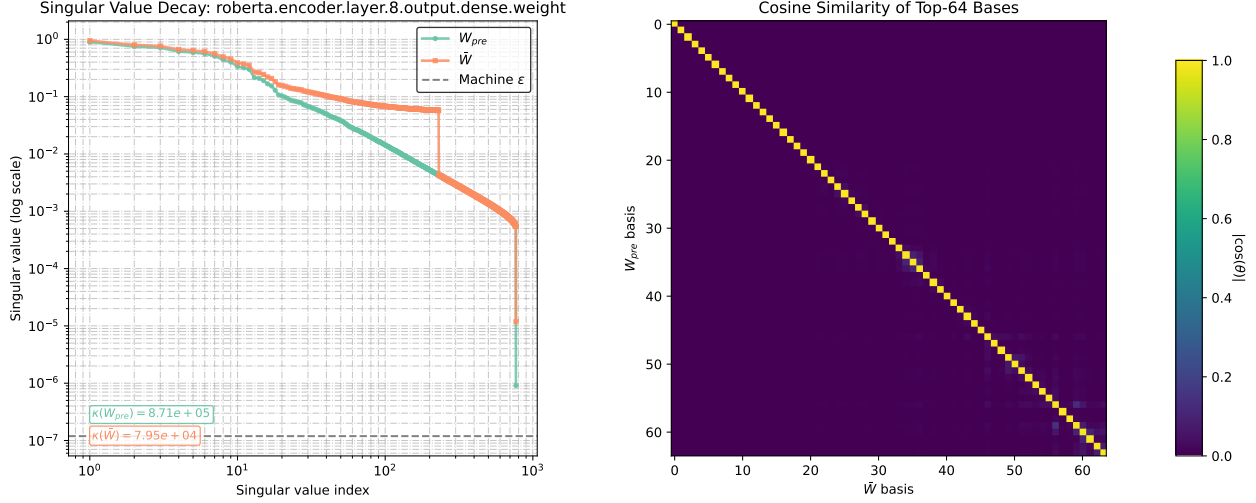
$$\bar{W}_{\text{pre}} = \left( \sum_{t \in [T]} W_t \hat{\Sigma}_{t,\text{reg}} \right) \left( \sum_{t \in [T]} \hat{\Sigma}_{t,\text{reg}} + \mathbf{C}_{\text{agg}} \right)^{-1}. \quad (10)$$

Unlike isotropic regularization, the *CSP* serves as a geometry-aware inductive bias that integrates inter-task structural consensus into the optimization, transforming regularization from a purely numerical device into an informative prior that promotes robustness and generalization.

### 4.4. Spectral refinement

Figure 2 illustrates a crucial phenomenon observed across high-heterogeneity benchmarks: even after trace normalization and the collective prior  $\mathbf{C}_{\text{agg}}$ , the preliminary closed-form solution  $\bar{W}_{\text{pre}}$  often remains *spectrally ill-conditioned*. As shown in the left panel of the figure, the top 5% singular values of  $\bar{W}_{\text{pre}}$  can carry more than 99% of the total Frobenius energy, indicating extreme spectral concentration and a condition number exceeding  $8.7 \times 10^5$ . Such spike-shaped spectra make the fused model highly sensitive to noise, suggesting that the matrix inversion in the closed-form update

Figure 2. Comparison between the preliminary closed-form solution  $\bar{W}_{\text{pre}}$  and the final merged model  $\bar{W}$ . **Left:** The singular value spectrum of  $\bar{W}_{\text{pre}}$  is extremely concentrated: the top 5% singular values capture more than 99% of the total energy, indicating severe spectral ill-conditioning. In contrast,  $\bar{W}$  exhibits a substantially flatter spectrum. **Right:** Despite this spectral imbalance, their leading eigenvectors are nearly identical (cosine similarity  $\approx 1$ ), showing that  $\bar{W}_{\text{pre}}$  already identifies the correct structural subspace. Spectral Refinement preserves this subspace while restoring a stable and expressive energy distribution.



unevenly suppresses the dominant consensus directions of the aggregated covariance.

However, the right panel reveals an important complementary fact: the principal directions of  $\bar{W}_{\text{pre}}$  are *nearly identical* to those of the final merged model  $\bar{W}$ . The leading eigenvectors exhibit cosine similarities close to 1, demonstrating that  $\bar{W}_{\text{pre}}$  already identifies the correct structural subspace; its deficiency lies not in direction but in its highly unbalanced spectral distribution. This observation motivates a refinement step that preserves the subspace geometry while restoring a more stable and expressive energy profile. To achieve this, we first compute the structural residual:

$$\Delta_{\text{res}} = \sum_{t \in [T]} W_t (\hat{\Sigma}_{t, \text{scaled}} - \bar{\Sigma}), \quad \bar{\Sigma} = \frac{1}{T} \sum_{t \in [T]} \hat{\Sigma}_{t, \text{reg}}. \quad (11)$$

which acts as a first-order correction to the closed-form solution, recovering structural variance that may be oversuppressed by the inversion. We then fuse this residual with the preliminary solution:  $\bar{W}_{\text{fused}} = \bar{W}_{\text{pre}} + \Delta_{\text{res}}$ . Applying SVD to the fused matrix,  $\bar{W}_{\text{fused}} = \mathbf{U}\mathbf{S}\mathbf{V}^{\top}$ , where  $\mathbf{S} = \text{diag}(\sigma_1, \sigma_2, \dots)$ , and re-weight the top- $k$  principal directions with their mean singular value,  $\sigma_{\text{iso}}$ :

$$\Delta W_{\text{refine}} = \sigma_{\text{iso}} \mathbf{U}_{:,1:k} \mathbf{V}_{:,1:k}^{\top}, \quad \sigma_{\text{iso}} = \frac{1}{k} \sum_{i=1}^k \sigma_i. \quad (12)$$

The final merged weight is obtained as:

$$\bar{W} = \bar{W}_{\text{pre}} + \Delta W_{\text{refine}}. \quad (13)$$

---

### Algorithm 1 ACE-Merging

---

**Require:** Pretrained weights  $W_0$ ; Expert weights  $\{W_t\}_{t \in [T]}$ ; Regularization strength  $\epsilon$ ; Heterogeneity threshold  $\tau$ ; Rank fraction  $k_{\text{frac}}$ .

**Ensure:** Merged weights  $\bar{W}$ .

1: **for** each layer  $l$  to be merged **do**

    ▷ **Stage 1: Adaptive Scaling**

- 2:     Compute task vectors  $\Delta W_t$  for all  $t$ .
- 3:     Compute metric  $\gamma$ , average trace  $\text{Tr}_{\text{avg}}$      Eq. (6)
- 4:     Compute scaled covariances  $\{\hat{\Sigma}_{t, \text{scaled}}\}$      Eq. (7)
- 5:     Compute regularized covariances  $\{\hat{\Sigma}_{t, \text{reg}}\}$      Eq. (8)

    ▷ **Stage 2: Structural Prior**

- 6:     Compute aggregate prior  $\mathbf{C}_{\text{agg}}$      Eq. (9)
- 7:     **if**  $\gamma > \tau$  **then**
- 8:         Normalize:  $\mathbf{C}_{\text{agg}} \leftarrow \mathbf{C}_{\text{agg}} / \text{Tr}_{\text{avg}}$ .
- 9:     **end if**

    ▷ **Stage 3: Fusion and Refinement**

- 10:     Compute preliminary merge  $\bar{W}_{\text{pre}}$      Eq. (10)
  - 11:     **if**  $\gamma > \tau$  **then**
  - 12:         Compute low-rank  $\Delta W_{\text{refine}}$      Eq. (12)
  - 13:          $\bar{W} \leftarrow \bar{W}_{\text{pre}} + \Delta W_{\text{refine}}$ .
  - 14:     **else**
  - 15:          $\bar{W} \leftarrow \bar{W}_{\text{pre}}$ .
  - 16:     **end if**
  - 17:     **end for**
  - 18:     **return**  $\bar{W} \leftarrow \{\bar{W}^{(l)}\}_l$
-

Table 1. Main results on visual benchmarks. We report the average absolute accuracy (%) across three ViT backbones (ViT-B/32, ViT-B/16, ViT-L/14) on task sets of increasing cardinality (8, 14, and 20). "Zero-shot" and "Fine-tuned" results serve as reference lower and upper bounds, respectively. The best performance among merging methods in each setting is highlighted in **bold**.

Method	ViT-B-32			ViT-B-16			ViT-L-14		
	8 tasks	14 tasks	20 tasks	8 tasks	14 tasks	20 tasks	8 tasks	14 tasks	20 tasks
Zero-shot	48.3	57.2	56.1	55.3	61.3	59.7	64.7	68.2	65.2
Fine-tuned	92.8	90.9	91.3	94.6	92.8	93.2	95.8	94.3	94.7
Weight Averaging [5]	66.3	64.3	61.0	72.2	69.5	65.3	79.6	76.7	71.6
Task Arithmetic [4]	70.8	65.3	60.5	75.4	70.5	65.8	84.9	79.4	74.0
Consensus TA [26]	75.0	70.4	65.4	79.4	74.4	69.8	86.3	82.2	79.0
CART [27]	84.7	79.5	76.3	88.3	84.1	80.5	92.6	88.7	87.9
TSV-M [19]	85.9	80.1	77.1	89.0	84.6	80.6	93.0	89.2	87.7
<b>ACE-Merging (Ours)</b>	<b>87.9</b>	<b>82.3</b>	<b>78.8</b>	<b>90.6</b>	<b>86.1</b>	<b>82.1</b>	<b>94.6</b>	<b>91.1</b>	<b>89.5</b>

Table 2. Performance on the GLUE benchmark for various merging methods applied to GPT-2. All scores are reported as accuracy, except for CoLA (Matthews Correlation). "Individual" represents the upper bound from single-task fine-tuned models.

Method	CoLA	MNLI	MRPC	QNLI	QQP	RTE	SST-2	Avg.
Individual	76.8	82.1	80.4	88.3	89.6	65.3	91.2	82.0
Weight Averaging [5]	55.0	55.1	51.0	57.6	76.7	44.8	52.5	56.1
Fisher Merging [6]	54.8	58.0	39.5	63.3	81.5	49.1	64.7	58.7
RegMean [7]	61.7	70.4	65.4	69.7	78.8	56.0	79.7	68.8
Task Arithmetic [4]	68.7	68.6	69.6	70.5	81.8	47.3	83.6	70.0
Ties-Merging [11]	68.4	71.4	68.4	69.6	82.4	47.7	81.8	70.0
TSV-M [19]	65.6	<b>75.4</b>	58.6	64.4	<b>86.2</b>	55.6	<b>85.7</b>	70.2
<b>ACE-Merging (Ours)</b>	<b>70.3</b>	69.9	<b>71.8</b>	<b>76.72</b>	79.0	<b>62.5</b>	<b>88.5</b>	<b>74.1</b>

#### 4.5. The ACE-Merging algorithm

The complete ACE-Merging procedure is summarized in Algorithm 1. For each layer, it operates in three main stages: first, it estimates the task heterogeneity to determine the merging strategy. Second, it computes a robust preliminary solution via our MAP framework. Finally, if significant heterogeneity is detected, it performs a targeted spectral refinement to correct for the inherent shrinkage bias.

### 5. Experiments

#### 5.1. Experimental setup

**Datasets.** For vision tasks, we evaluate on three vision benchmarks with cardinalities of 8, 14, and 20. These benchmarks are constructed by progressively extending the task selection protocol of [19]. The 8-task benchmark serves as our base setting and includes Cars [28], DTD [29], EuroSAT [30], GTSRB [31], MNIST [32], RESISC45 [33], SUN397 [34], and SVHN [35]. The 14-task benchmark adds CIFAR100 [36], STL10 [37], Flowers102 [38], OxfordIIITPet [39], PCAM [40], and FER2013 [41]. The 20-task benchmark further adds EMNIST [42], CIFAR10 [36], Food101 [43], FashionMNIST [44], RenderedSST2 [45],

and KMNIST [46]. For language tasks, our evaluation is based on the widely used GLUE benchmark [47], and we report results on its eight core tasks: CoLA, SST-2, MRPC, STS-B, QQP, QNLI, MNLI, and RTE.

**Models.** For vision tasks, we adopt CLIP-derived Vision Transformers (ViTs) [48, 49], evaluating models at multiple scales including ViT-B/32, ViT-B/16, and ViT-L/14. The corresponding fine-tuned checkpoints are taken from the TSV-M suite [19].

For language tasks, we consider both the RoBERTa [50] and GPT-2 [51] model families, conducting experiments on RoBERTa-Base, RoBERTa-Large, and GPT-2. RoBERTa checkpoints are sourced from the Twin-Merging benchmark [52], while GPT-2 checkpoints are obtained from the FusionBench benchmark [53]. Additionally, we also evaluate our method on the Llama-3B-Instruct [54] and report the results in the Appendix B.

**Baselines.** Our evaluation includes comparisons with numerous recent approaches reported across different tasks. For consistency and brevity, we restrict our detailed comparisons to the state-of-the-art data-free methods most com-

Table 3. Normalized performance on the GLUE benchmark for RoBERTa-Base and RoBERTa-Large. The average score is reported, with the red triangle indicating the improvement over the best baseline (Ties-Merging w/ DARE). Best results in each column are in **bold**.

Model	Method	CoLA	SST-2	MRPC	STS-B	QQP	QNLI	MNLI	RTE	Avg.
RoBERTa-Base	Pre-trained	0.0	53.8	85.0	4.0	37.5	53.1	37.1	71.2	41.7
	Individual	100.0	100.0	100.0	100.0	100.0	100.0	100.0	100.0	100.0
	Weight Averaging [5]	0.0	59.2	85.8	47.0	45.4	63.9	48.0	71.2	52.6
	Task Arithmetic [4]	8.4	88.3	89.6	32.8	82.0	85.4	75.5	80.4	67.8
	Ties-Mergin [11] g	31.8	88.9	86.2	10.9	61.1	85.9	83.0	69.6	64.7
	Task Arithmetic (w/ DARE) [14]	0.0	88.1	86.6	30.2	84.3	79.1	64.0	77.2	63.7
	Ties-Merging (w/ DARE) [14]	11.8	95.5	85.8	9.4	86.8	88.7	83.1	65.6	65.6
	WUDI-Merging [23]	81.8	<b>98.3</b>	78.7	60.5	92.7	<b>90.5</b>	<b>93.3</b>	86.4	85.3
<b>ACE-Merging (Ours)</b>		<b>97.3</b>	97.6	<b>93.9</b>	<b>71.1</b>	<b>88.3</b>	88.2	91.5	<b>95.1</b>	<b>90.4</b>
RoBERTa-Large	Pre-trained	0.0	51.5	40.9	20.9	36.4	56.0	37.6	62.4	38.2
	Individual	100.0	100.0	100.0	100.0	100.0	100.0	100.0	100.0	100.0
	Weight Averaging	7.4	55.1	84.2	46.3	56.7	73.8	35.8	66.7	53.3
	Task Arithmetic	7.4	86.1	86.8	78.0	90.7	77.0	73.3	67.6	70.9
	Ties-Merging	42.7	78.1	85.2	51.7	89.9	81.9	79.7	70.0	72.4
	Task Arithmetic (w/ DARE)	4.1	85.2	85.8	71.6	91.3	85.6	75.2	68.1	70.9
	Ties-Merging (w/ DARE)	2.9	90.4	86.8	75.4	92.4	86.4	79.0	69.1	72.8
	WUDI-Merging	82.2	98.7	87.3	81.4	94.6	96.6	<b>93.4</b>	77.1	88.8
<b>ACE-Merging (Ours)</b>		<b>87.1</b>	<b>99.2</b>	<b>92.3</b>	<b>82.1</b>	<b>95.6</b>	<b>97.9</b>	92.6	<b>86.7</b>	<b>91.7</b>

monly used as baselines in prior studies. This enables a fair and representative assessment while keeping the benchmark analysis compact.

**Experiment details.** For our method, we use consistent hyperparameters across all experiments. The heterogeneity threshold is fixed to  $\tau = 0.3$ , and we set the rank fraction  $k_{\text{frac}} = 0.3$ , indicating that the spectral refinement step retains the top  $k = k_{\text{frac}} \times \min(d_{\text{in}}, d_{\text{out}})$  singular components. The regularization strength  $\epsilon$  is adapted to the model family, set to  $4 \times 10^{-2}$  for GPT-2,  $2 \times 10^{-4}$  for RoBERTa-Base, and  $1 \times 10^{-5}$  for all other models.

## 5.2. Main results

We comprehensively evaluate ACE-Merging across a suite of vision and language benchmarks. As shown in Table 1, Table 2, and Table 3, our method consistently outperforms various baseline methods in all evaluation settings.

**Vision task performance.** Table 1 summarizes the average absolute accuracy on the 8-, 14-, and 20-task visual benchmarks. The results clearly indicate that ACE-Merging achieves state-of-the-art (SOTA) performance across all nine settings. Notably, the performance gap between ACE-Merging and prior SOTA methods, such as CART and TSV-M, widens as both model scale (from ViT-B/32 to ViT-L/14) and task cardinality increase. For instance, in the most challenging 20-task setting on

ViT-L/14, our method achieves 89.5 accuracy, surpassing the next best method by nearly 2 absolute points. This strongly demonstrates that ACE-Merging provides robust and scalable performance gains, regardless of model capacity or task complexity.

**Language task performance.** Our experiments on language models further corroborate the superiority and generalization capabilities of ACE-Merging.

On GPT-2 (Table 2), ACE-Merging achieves an average score of 74.1%, decisively outperforming all baselines, including Ties-Merging 70.0% and the SVD-based TSV-M 70.2, by a large margin of over 4 absolute points.

The results on RoBERTa models (Table 3) are equally impressive. On RoBERTa-Base, our method attains a normalized average score of 90.4%, which is over 5 points higher than the strong WUDI-Merging baseline (85.3%). This advantage is sustained on RoBERTa-Large, where ACE-Merging achieves 91.7%, nearly 3 points ahead of WUDI-Merging (88.8%). These consistent SOTA results across diverse language architectures and scales confirm that our method is not a model-specific optimization but a fundamental and broadly applicable solution to the model merging problem.

## 5.3. Ablation study

To understand the contribution of each component within ACE-Merging, we conduct a detailed ablation study.

Table 4. Ablation study of ACE-Merging components. We report the average score (%) on RoBERTa-Large (GLUE), GPT-2 (GLUE), and ViT-B/16 (8 tasks). The best performing configuration for each model is marked in bold.

#	Method Configuration	RoBERTa-L	GPT-2	ViT-B/16
E1	Basic Closed-form	80.05	68.72	89.91
E2	+ Adaptive $\epsilon$	88.04	71.50	89.91
E3	+ Aggregate Prior ( $\Lambda_{\text{agg}}$ )	86.79	71.51	<b>90.60</b>
E4	+ Spectral Refinement	<b>91.68</b>	<b>74.09</b>	<b>90.60</b>

Table 5. Effect of the heterogeneity threshold  $\gamma$  (fixed  $k_{\text{frac}} = 0.3$ ). Average accuracy (%) on RoBERTa-Large (GLUE) and GPT-2 (FusionBench).

$\gamma$	RoBERTa-Large	GPT-2
0.1	<b>92.22</b>	73.96
0.2	92.21	73.96
0.3	91.68	<b>74.09</b>
0.4	89.07	71.74
0.5	88.09	69.35

Starting from a basic closed-form baseline (E1), we progressively add three modules: adaptive regularization (E2), the empirical Bayes aggregate prior (E3), and the spectral refinement stage (E4). Table 4 summarizes the results on RoBERTa-Large, GPT-2, and ViT-B/16 (8 tasks).

**Analysis on language models.** On both RoBERTa-Large and GPT-2, the results show clear cumulative improvements. The introduction of adaptive regularization (E2) gives the largest gain, improving RoBERTa-Large by almost eight points. This confirms that adjusting the effective regularization according to task heterogeneity is essential. Adding the aggregate prior (E3) produces a small fluctuation, which is resolved when the spectral refinement stage (E4) is included. The final configuration achieves the best performance on all models. This result indicates that the three modules complement each other and together produce a stable and accurate closed-form solution.

**Analysis on vision models.** For ViT-B/16, the measured heterogeneity  $\gamma$  across the eight tasks stays below the activation threshold  $\tau = 0.3$  for all layers. As a result, ACE-Merging correctly skips the adaptive and spectral stages. This behavior is consistent with Table 4, where E2 matches E1 and E4 matches E3. The results confirm that the  $\gamma$ -based gate works as an effective switch that activates correction only when large task differences are detected. The improvement from E2 to E3 shows that the aggregate prior still provides a steady benefit even when heterogeneity is low.

Table 6. Effect of the spectral rank fraction  $k_{\text{frac}}$  under fixed heterogeneity threshold  $\gamma = 0.3$ . Average accuracy (%) on RoBERTa-Large (GLUE) and GPT-2 (FusionBench).

$k_{\text{frac}}$	RoBERTa-Large	GPT-2
0.1	90.71	<b>74.17</b>
0.2	91.55	73.88
0.3	<b>91.68</b>	74.09
0.4	91.61	74.06
0.5	91.45	73.78
0.6	91.17	73.71

**Sensitivity analysis.** Tables 5 and 6 show the sensitivity of ACE-Merging to the heterogeneity threshold  $\gamma$  and the spectral rank fraction  $k_{\text{frac}}$ . The performance remains stable for  $\gamma$  between 0.1 and 0.3 and for  $k_{\text{frac}}$  between 0.1 and 0.5. This indicates that the method is robust to moderate changes in these parameters. The regularization strength  $\epsilon$  plays a more critical role because it directly controls the balance between stability and fidelity. A possible direction for future work is to design an automatic procedure to estimate an optimal  $\epsilon$  from model statistics.

**Summary.** The ablation and sensitivity results show that each module in ACE-Merging has a distinct and complementary function. Adaptive regularization improves numerical stability. The aggregate prior enforces consistent structure across tasks. Spectral refinement restores balanced singular spectra and alignment. At the same time, the framework is robust to a wide range of  $\gamma$  and  $k_{\text{frac}}$  values, confirming its reliability and scalability in practice.

## 6. Conclusion

In this work, we tackle the challenge of data-free model merging under substantial inter-task heterogeneity. We introduce ACE-Merging, a unified framework that integrates adaptive normalization, a collective structural prior, and a spectral refinement stage to effectively synthesize shared knowledge while preserving salient task-specific structure. Extensive experiments across diverse vision and language benchmarks demonstrate that ACE-Merging consistently achieves state-of-the-art performance. Its advantages become increasingly pronounced as model scale and task diversity grow, highlighting the robustness and scalability of the proposed approach. A promising direction for future work is to make the regularization strength  $\epsilon$  input-aware rather than a single global constant. We hope that ACE-Merging serves both as a practical tool and as a conceptual foundation for advancing research in scalable, data-free model fusion.

## References

- [1] Ashish Vaswani, Noam Shazeer, Niki Parmar, Jakob Uszkoreit, Llion Jones, Aidan N Gomez, Łukasz Kaiser, and Illia Polosukhin. Attention is all you need. *Advances in neural information processing systems*, 30, 2017. 1
- [2] Jacob Devlin, Ming-Wei Chang, Kenton Lee, and Kristina Toutanova. Bert: Pre-training of deep bidirectional transformers for language understanding. In *Proceedings of the 2019 conference of the North American chapter of the association for computational linguistics: human language technologies, volume 1 (long and short papers)*, pages 4171–4186, 2019. 1
- [3] Rich Caruana. Multitask learning. *Machine learning*, 28(1):41–75, 1997. 1
- [4] Gabriel Ilharco, Marco Tulio Ribeiro, Mitchell Wortsman, Ludwig Schmidt, Hannaneh Hajishirzi, and Ali Farhadi. Editing models with task arithmetic. In *The Eleventh International Conference on Learning Representations*, 2023. 1, 2, 6, 7
- [5] Mitchell Wortsman, Gabriel Ilharco, Samir Yitzhak Gadre, Rebecca Roelofs, Raphael Gontijo-Lopes, Ari S. Morcos, Hongseok Namkoong, Ali Farhadi, Yair Carmon, Simon Kornblith, and Ludwig Schmidt. Model soups: averaging weights of multiple fine-tuned models improves accuracy without increasing inference time. *ArXiv*, abs/2203.05482, 2022. 1, 3, 6, 7
- [6] Michael S Matena and Colin A Raffel. Merging models with fisher-weighted averaging. *Advances in Neural Information Processing Systems*, 35:17703–17716, 2022. 1, 2, 6
- [7] Xisen Jin, Xiang Ren, Daniel Preotiuc-Pietro, and Pengxiang Cheng. Dataless knowledge fusion by merging weights of language models. *arXiv preprint arXiv:2212.09849*, 2022. 6
- [8] The-Hai Nguyen, Dang Huu-Tien, Takeshi Suzuki, and Le-Minh Nguyen. Regmean++: Enhancing effectiveness and generalization of regression mean for model merging. *arXiv preprint arXiv:2508.03121*, 2025. 1, 2
- [9] Enneng Yang, Zhenyi Wang, Li Shen, Shiwei Liu, Guibing Guo, Xingwei Wang, and Dacheng Tao. Adamerging: Adaptive model merging for multi-task learning. *arXiv preprint arXiv:2310.02575*, 2023. 1, 2
- [10] Chenyu Huang, Peng Ye, Tao Chen, Tong He, Xiangyu Yue, and Wanli Ouyang. Emr-merging: Tuning-free high-performance model merging. *Advances in Neural Information Processing Systems*, 37:122741–122769, 2024. 1, 2
- [11] Prateek Yadav, Derek Tam, Leshem Choshen, Colin A Raffel, and Mohit Bansal. Ties-merging: Resolving interference when merging models. *Advances in Neural Information Processing Systems*, 36:7093–7115, 2023. 1, 2, 6, 7
- [12] Chongjie Si, Kangtao Lv, Jingjing Jiang, Yadao Wang, Yongwei Wang, Xiaokang Yang, Wenbo Su, Bo Zheng, and Wei Shen. Nan: A training-free solution to coefficient estimation in model merging. *arXiv preprint arXiv:2505.16148*, 2025.
- [13] Shenghe Zheng and Hongzhi Wang. Free-merging: Fourier transform for efficient model merging. In *Proceedings of the IEEE/CVF International Conference on Computer Vision*, pages 3863–3873, 2025. 2
- [14] Le Yu, Bowen Yu, Haiyang Yu, Fei Huang, and Yongbin Li. Language models are super mario: Absorbing abilities from homologous models as a free lunch. In *Forty-first International Conference on Machine Learning*, 2024. 1, 2, 7
- [15] Sanwoo Lee, Jiahao Liu, Qifan Wang, Jingang Wang, Xunliang Cai, and Yunfang Wu. Dynamic fisher-weighted model merging via bayesian optimization. *arXiv preprint arXiv:2504.18992*, 2025. 2
- [16] Ryo Bertolissi, Jonas Hübner, Ido Hakimi, and Andreas Krause. Local mixtures of experts: Essentially free test-time training via model merging. *arXiv preprint arXiv:2505.14136*, 2025. 2
- [17] Zihuan Qiu, Yi Xu, Chiyuan He, Fanman Meng, Linfeng Xu, Qingbo Wu, and Hongliang Li. Mingle: Mixtures of null-space gated low-rank experts for test-time continual model merging. *arXiv preprint arXiv:2505.11883*, 2025. 2
- [18] Pala Tej Deep, Rishabh Bhardwaj, and Soujanya Poria. Della-merging: Reducing interference in model merging through magnitude-based sampling. *arXiv preprint arXiv:2406.11617*, 2024. 2
- [19] Antonio Andrea Gargiulo, Donato Crisostomi, Maria Sofia Bucarelli, Simone Scardapane, Fabrizio Silvestri, and Emanuele Rodola. Task singular vectors: Reducing task interference in model merging. In *Proceedings of the Computer Vision and Pattern Recognition Conference*, pages 18695–18705, 2025. 2, 6, 7
- [20] Daniel Marczak, Simone Magistri, Sebastian Cygert, Bartłomiej Twardowski, Andrew D. Bagdanov, and Joost van de Weijer. No task left behind: Isotropic model merging with common and task-specific subspaces. In *Forty-second International Conference on Machine Learning*, 2025.
- [21] George Stoica, Pratik Ramesh, Boglarka Ecsedi, Leshem Choshen, and Judy Hoffman. Model merging with svd to tie the knots. *arXiv preprint arXiv:2410.19735*, 2024.
- [22] Aniello Panariello, Daniel Marczak, Simone Magistri, Angelo Porrello, Bartłomiej Twardowski, Andrew D. Bagdanov, Simone Calderara, and Joost van de Weijer. Accurate and efficient low-rank model merging in core space. *ArXiv*, abs/2509.17786, 2025. 2
- [23] Runxi Cheng, Feng Xiong, Yongxian Wei, Wanyun Zhu, and Chun Yuan. Whoever started the interference should end it: Guiding data-free model merging via task vectors. *arXiv preprint arXiv:2503.08099*, 2025. 2, 3, 7
- [24] Anton Razzhigaev, Matvey Mikhalechuk, Elizaveta Goncharova, Nikolai Gerasimenko, Ivan Oseledets, Denis Dimitrov, and Andrey Kuznetsov. Your transformer is secretly linear. *arXiv preprint arXiv:2405.12250*, 2024. 3
- [25] Wei Huang, Anda Cheng, and Yingui Wang. Mitigating catastrophic forgetting in large language models with forgetting-aware pruning. *ArXiv*, abs/2509.08255, 2025. 3
- [26] Ke Wang, Nikolaos Dimitriadis, Guillermo Ortiz-Jiménez, Francois Fleuret, and Pascal Frossard. Localizing task information for improved model merging and compression. *ArXiv*, abs/2405.07813, 2024. 6
- [27] Jiho Choi, Donggyun Kim, Chanhyuk Lee, and Seunghoon Hong. Revisiting weight averaging for model merging. *ArXiv*, abs/2412.12153, 2024. 6

- [28] Jonathan Krause, Michael Stark, Jia Deng, and Li Fei-Fei. 3d object representations for fine-grained categorization. In *Proceedings of the IEEE international conference on computer vision workshops*, pages 554–561, 2013. 6
- [29] Mircea Cimpoi, Subhransu Maji, Iasonas Kokkinos, Sammy Mohamed, and Andrea Vedaldi. Describing textures in the wild. In *Proceedings of the IEEE conference on computer vision and pattern recognition*, pages 3606–3613, 2014. 6
- [30] Patrick Helber, Benjamin Bischke, Andreas Dengel, and Damian Borth. Eurosat: A novel dataset and deep learning benchmark for land use and land cover classification. *IEEE Journal of Selected Topics in Applied Earth Observations and Remote Sensing*, 12(7):2217–2226, 2019. 6
- [31] Johannes Stallkamp, Marc Schlipsing, Jan Salmen, and Christian Igel. The german traffic sign recognition benchmark: a multi-class classification competition. In *The 2011 international joint conference on neural networks*, pages 1453–1460. IEEE, 2011. 6
- [32] Yann LeCun, Léon Bottou, Yoshua Bengio, and Patrick Haffner. Gradient-based learning applied to document recognition. *Proceedings of the IEEE*, 86(11):2278–2324, 2002. 6
- [33] Gong Cheng, Junwei Han, and Xiaoqiang Lu. Remote sensing image scene classification: Benchmark and state of the art. *Proceedings of the IEEE*, 105(10):1865–1883, 2017. 6
- [34] Jianxiong Xiao, Krista A Ehinger, James Hays, Antonio Torralba, and Aude Oliva. Sun database: Exploring a large collection of scene categories. *International Journal of Computer Vision*, 119(1):3–22, 2016. 6
- [35] Yuval Netzer, Tao Wang, Adam Coates, Alessandro Bisacco, Baolin Wu, Andrew Y Ng, et al. Reading digits in natural images with unsupervised feature learning. In *NIPS workshop on deep learning and unsupervised feature learning*, volume 2011, page 7. Granada, 2011. 6
- [36] Alex Krizhevsky and Geoffrey Hinton. Learning multiple layers of features from tiny images. Technical Report TR-2009, University of Toronto, Toronto, Ontario, 2009. 6
- [37] Adam Coates, Andrew Ng, and Honglak Lee. An analysis of single-layer networks in unsupervised feature learning. In *Proceedings of the fourteenth international conference on artificial intelligence and statistics*, pages 215–223. JMLR Workshop and Conference Proceedings, 2011. 6
- [38] Maria-Elena Nilsback and Andrew Zisserman. Automated flower classification over a large number of classes. In *2008 Sixth Indian conference on computer vision, graphics & image processing*, pages 722–729. IEEE, 2008. 6
- [39] Omkar M Parkhi, Andrea Vedaldi, Andrew Zisserman, and CV Jawahar. Cats and dogs. In *2012 IEEE conference on computer vision and pattern recognition*, pages 3498–3505. IEEE, 2012. 6
- [40] Bastiaan S Veeling, Jasper Linmans, Jim Winkens, Taco Cohen, and Max Welling. Rotation equivariant cnns for digital pathology. In *International Conference on Medical image computing and computer-assisted intervention*, pages 210–218. Springer, 2018. 6
- [41] Ian J Goodfellow, Dumitru Erhan, Pierre Luc Carrier, Aaron Courville, Mehdi Mirza, Ben Hamner, Will Cukierski, Yichuan Tang, David Thaler, Dong-Hyun Lee, et al. Challenges in representation learning: A report on three machine learning contests. In *International conference on neural information processing*, pages 117–124. Springer, 2013. 6
- [42] Gregory Cohen, Saeed Afshar, Jonathan Tapson, and Andre Van Schaik. Emnist: Extending mnist to handwritten letters. In *2017 international joint conference on neural networks (IJCNN)*, pages 2921–2926. IEEE, 2017. 6
- [43] Lukas Bossard, Matthieu Guillaumin, and Luc Van Gool. Food-101—mining discriminative components with random forests. In *European conference on computer vision*, pages 446–461. Springer, 2014. 6
- [44] Han Xiao, Kashif Rasul, and Roland Vollgraf. Fashion-mnist: a novel image dataset for benchmarking machine learning algorithms. *arXiv preprint arXiv:1708.07747*, 2017. 6
- [45] Richard Socher, Alex Perelygin, Jean Wu, Jason Chuang, Christopher D Manning, Andrew Y Ng, and Christopher Potts. Recursive deep models for semantic compositionality over a sentiment treebank. In *Proceedings of the 2013 conference on empirical methods in natural language processing*, pages 1631–1642, 2013. 6
- [46] Tarin Clanuwat, Mikel Bober-Irizar, Asanobu Kitamoto, Alex Lamb, Kazuaki Yamamoto, and David Ha. Deep learning for classical japanese literature. *arXiv preprint arXiv:1812.01718*, 2018. 6
- [47] Alex Wang, Amanpreet Singh, Julian Michael, Felix Hill, Omer Levy, and Samuel Bowman. Glue: A multi-task benchmark and analysis platform for natural language understanding. In *Proceedings of the 2018 EMNLP workshop BlackboxNLP: Analyzing and interpreting neural networks for NLP*, pages 353–355, 2018. 6
- [48] Alexey Dosovitskiy. An image is worth 16x16 words: Transformers for image recognition at scale. *arXiv preprint arXiv:2010.11929*, 2020. 6
- [49] Alec Radford, Jong Wook Kim, Chris Hallacy, Aditya Ramesh, Gabriel Goh, Sandhini Agarwal, Girish Sastry, Amanda Askell, Pamela Mishkin, Jack Clark, et al. Learning transferable visual models from natural language supervision. In *International conference on machine learning*, pages 8748–8763. PmLR, 2021. 6
- [50] Yinhan Liu, Myle Ott, Naman Goyal, Jingfei Du, Mandar Joshi, Danqi Chen, Omer Levy, Mike Lewis, Luke Zettlemoyer, and Veselin Stoyanov. Roberta: A robustly optimized bert pretraining approach. *ArXiv*, abs/1907.11692, 2019. 6
- [51] Alec Radford, Jeffrey Wu, Rewon Child, David Luan, Dario Amodei, Ilya Sutskever, et al. Language models are unsupervised multitask learners. *OpenAI blog*, 1(8):9, 2019. 6
- [52] Zhenyi Lu, Chenghao Fan, Wei Wei, Xiaoye Qu, Danyang Chen, and Yu Cheng. Twin-merging: Dynamic integration of modular expertise in model merging. *Advances in Neural Information Processing Systems*, 37:78905–78935, 2024. 6
- [53] Anke Tang, Li Shen, Yong Luo, Han Hu, Bo Du, and Dacheng Tao. Fusionbench: A comprehensive benchmark of deep model fusion. *arXiv preprint arXiv:2406.03280*, 2024. 6

- [54] Hugo Touvron, Thibaut Lavril, Gautier Izacard, Xavier Martinet, Marie-Anne Lachaux, Timothée Lacroix, Baptiste Rozière, Naman Goyal, Eric Hambro, Faisal Azhar, Aurélien Rodriguez, Armand Joulin, Edouard Grave, and Guillaume Lample. Llama: Open and efficient foundation language models. *ArXiv*, abs/2302.13971, 2023. [6](#)

## A. Theoretical Derivations

### A.1. Derivation of the Quadratic Objective

In this section, we provide the full derivation showing how the objective in Eq. (1) of the main paper reduces to the quadratic form in Eq. (2) under the standard linearization assumption.

Recall that the merging objective is

$$\min_{\bar{W}} \sum_{t \in [T]} \mathbb{E}_{x \sim D_t} \|f(\bar{W}, x) - f(W_t, x)\|_2^2.$$

Let us first consider the inner term of the summation for a single task  $t$ . Following common practice and our analysis in Section 3.2, we linearize the forward pass as  $f(W, x) \approx Wx$ . This approximation, supported by the local linearity of Transformer layers during fine-tuning, allows us to simplify the term as follows:

$$\mathbb{E}_{x \sim D_t} \|f(\bar{W}, x) - f(W_t, x)\|_2^2 \approx \mathbb{E}_{x \sim D_t} \|(\bar{W} - W_t)x\|_2^2. \quad (14)$$

For any matrix  $A$  and vector  $x$ , we have the identity  $\|Ax\|_2^2 = x^\top A^\top Ax$ . Applying this within the expectation yields:

$$\mathbb{E}_{x \sim D_t} \|(\bar{W} - W_t)x\|_2^2 = \mathbb{E}_{x \sim D_t} [x^\top (\bar{W} - W_t)^\top (\bar{W} - W_t)x]. \quad (15)$$

Let us analyze the dimensions of the term inside the expectation. The weight matrices are  $\bar{W}, W_t \in \mathbb{R}^{d_{\text{out}} \times d_{\text{in}}}$ , and the input vector is  $x \in \mathbb{R}^{d_{\text{in}} \times 1}$ . Let  $\Delta W = \bar{W} - W_t$ . The dimensions are as follows:

$$\underbrace{x^\top}_{1 \times d_{\text{in}}} \underbrace{(\Delta W)^\top}_{d_{\text{in}} \times d_{\text{out}}} \underbrace{(\Delta W)}_{d_{\text{out}} \times d_{\text{in}}} \underbrace{x}_{d_{\text{in}} \times 1}.$$

The resulting product has dimensions  $(1 \times d_{\text{in}}) \cdot (d_{\text{in}} \times d_{\text{out}}) \cdot (d_{\text{out}} \times d_{\text{in}}) \cdot (d_{\text{in}} \times 1) = (1 \times 1)$ , which is a scalar.

The key insight is that any scalar is equal to its own trace. Using this fact, along with the linearity of both trace and expectation and the cyclic property of the trace ( $\text{Tr}(ABC) = \text{Tr}(CAB)$ ), we can rewrite the expression:

$$\begin{aligned} \mathbb{E}_{x \sim D_t} [\dots] &= \mathbb{E}_{x \sim D_t} \left[ \text{Tr} \left( x^\top (\bar{W} - W_t)^\top (\bar{W} - W_t) x \right) \right] \\ &= \text{Tr} \left( \mathbb{E}_{x \sim D_t} [(\bar{W} - W_t) x x^\top (\bar{W} - W_t)^\top] \right) \\ &= \text{Tr} \left( (\bar{W} - W_t) \mathbb{E}_{x \sim D_t} [x x^\top] (\bar{W} - W_t)^\top \right). \end{aligned} \quad (16)$$

By applying the cyclic property one final time,  $\text{Tr}(ABC) = \text{Tr}(CAB)$ , we arrive at the symmetric form:

$$\mathbb{E}_{x \sim D_t} [\dots] = \text{Tr} \left[ (\bar{W} - W_t) \left( \mathbb{E}_{x \sim D_t} [x x^\top] \right) (\bar{W} - W_t)^\top \right]. \quad (17)$$

Define the input covariance matrix of task  $t$  as

$$\Sigma_t = \mathbb{E}_{x \sim D_t} [x x^\top].$$

We obtain

$$\mathbb{E}_{x \sim D_t} \|(\bar{W} - W_t)x\|_2^2 = \text{Tr} \left[ (\bar{W} - W_t) \Sigma_t (\bar{W} - W_t)^\top \right]. \quad (18)$$

Summing over all tasks  $t \in [T]$ , we arrive at

$$\mathcal{L}(\bar{W}) = \sum_{t=1}^T \text{Tr} \left[ (\bar{W} - W_t) \Sigma_t (\bar{W} - W_t)^\top \right], \quad (19)$$

which is exactly Eq. (2) in the main paper.

## A.2. Derivation of the Closed-Form Solution

In this section, we derive the closed-form solution for the optimal merged weights  $\bar{W}$  by minimizing the quadratic objective function from Eq. (2).

To find the minimum, we compute the gradient of  $\mathcal{L}(\bar{W})$  with respect to the matrix  $\bar{W}$  and set it to zero. First, let's expand the term inside the trace:

$$\begin{aligned} (\bar{W} - W_t)\Sigma_t(\bar{W} - W_t)^\top &= (\bar{W} - W_t)\Sigma_t(\bar{W}^\top - W_t^\top) \\ &= \bar{W}\Sigma_t\bar{W}^\top - \bar{W}\Sigma_tW_t^\top - W_t\Sigma_t\bar{W}^\top + W_t\Sigma_tW_t^\top. \end{aligned} \quad (20)$$

Using the linearity of the trace and the sum, we can differentiate the loss term by term with respect to  $\bar{W}$ . We use the following standard matrix calculus identities for the gradient of a trace:

- $\nabla_X \text{Tr}(XAX^\top) = X(A + A^\top)$
- $\nabla_X \text{Tr}(XB) = B^\top$
- $\nabla_X \text{Tr}(AX^\top) = A$

Given that the covariance matrix  $\Sigma_t$  is symmetric (i.e.,  $\Sigma_t = \Sigma_t^\top$ ), the first identity simplifies to  $\nabla_X \text{Tr}(X\Sigma_tX^\top) = 2X\Sigma_t$ . Applying these rules, the gradient of the loss function is:

$$\begin{aligned} \nabla_{\bar{W}}\mathcal{L}(\bar{W}) &= \nabla_{\bar{W}} \sum_{t \in [T]} \text{Tr} [\bar{W}\Sigma_t\bar{W}^\top - \bar{W}\Sigma_tW_t^\top - W_t\Sigma_t\bar{W}^\top + W_t\Sigma_tW_t^\top] \\ &= \sum_{t \in [T]} \nabla_{\bar{W}} \text{Tr} [\bar{W}\Sigma_t\bar{W}^\top - \bar{W}\Sigma_tW_t^\top - W_t\Sigma_t\bar{W}^\top] \\ &= \sum_{t \in [T]} (2\bar{W}\Sigma_t - (\Sigma_tW_t^\top)^\top - W_t\Sigma_t) \\ &= \sum_{t \in [T]} (2\bar{W}\Sigma_t - W_t\Sigma_t^\top - W_t\Sigma_t) \\ &= \sum_{t \in [T]} (2\bar{W}\Sigma_t - 2W_t\Sigma_t) \quad (\text{since } \Sigma_t = \Sigma_t^\top) \\ &= 2 \sum_{t \in [T]} (\bar{W}\Sigma_t - W_t\Sigma_t). \end{aligned} \quad (21)$$

Setting the gradient to zero to find the minimum:

$$\begin{aligned} 2 \sum_{t \in [T]} (\bar{W}\Sigma_t - W_t\Sigma_t) &= 0 \\ \sum_{t \in [T]} \bar{W}\Sigma_t &= \sum_{t \in [T]} W_t\Sigma_t. \end{aligned} \quad (22)$$

Since  $\bar{W}$  is common to all terms in the left-hand summation, we can factor it out:

$$\bar{W} \left( \sum_{t \in [T]} \Sigma_t \right) = \sum_{t \in [T]} W_t\Sigma_t. \quad (23)$$

Finally, to isolate  $\bar{W}$ , we right-multiply both sides by the inverse of the aggregated covariance matrix:

$$\bar{W} = \left( \sum_{t \in [T]} W_t\Sigma_t \right) \left( \sum_{t \in [T]} \Sigma_t \right)^{-1}. \quad (24)$$

This gives us the closed-form solution for the optimal merged weights, as presented in the main paper.

### A.3. Proof of Theorem 1

We restate the setting and make our assumptions explicit. Let  $W_0 \in \mathbb{R}^{d_{\text{out}} \times d_{\text{in}}}$  be the pretrained weights, and let  $W_t$  denote the task-specific weights obtained by fine-tuning on task  $t$  over the dataset  $\mathcal{D}_t = \{(x_i, y_i)\}_{i=1}^{N_t}$ . We write the total weight displacement as  $\Delta W_t = W_t - W_0$ .

**Assumptions.** We use the following assumptions throughout the derivation:

(A1) **Linearized squared-loss gradient.** The loss is  $\mathcal{L}_t(x, y; W) = \|Wx - y\|_2^2$ , and the fine-tuning trajectory stays in a neighborhood of  $W_0$  so that

$$\nabla_W \mathcal{L}_t(x, y; W_0) = 2(W_0 x - y) x^\top = 2e x^\top,$$

where  $e = W_0 x - y$  is the residual.

(A2) **i.i.d. samples.** Training pairs  $(x_i, y_i)$  are drawn i.i.d. from  $\mathcal{D}_t$ .

(A3) **Locally unbiased pretrained model.** The pretrained model satisfies

$$\mathbb{E}_{(x,y) \sim \mathcal{D}_t} [e x^\top] = 0.$$

(A4) **Factorized second-order structure.** The residual energy  $e^\top e$  is uncorrelated with  $x x^\top$ :

$$\mathbb{E}[(e^\top e) x x^\top] = \mathbb{E}[e^\top e] \mathbb{E}[x x^\top] = \sigma_{e, \text{total}}^2 \Sigma_t,$$

where  $\Sigma_t = \mathbb{E}[x x^\top]$ .

Assumption (A1) is standard for local analysis of squared loss; (A2) is the usual sampling assumption; (A3) corresponds to  $W_0$  being a local stationary point for task  $t$ ; and (A4) is a mild independence assumption aligning the second moment of the updates with the input covariance.

**Step 1: Linearized expression for  $\Delta W_t$ .** Under (A1), a single SGD step on  $(x_i, y_i)$  with learning rate  $\eta$  yields

$$\Delta W^{(i)} = -\eta \nabla_W \mathcal{L}_t(x_i, y_i; W_0) = -2\eta e_i x_i^\top,$$

with  $e_i = W_0 x_i - y_i$ . Summing over all  $N_t$  samples gives

$$\Delta W_t = \sum_{i=1}^{N_t} \Delta W^{(i)} = -2\eta \sum_{i=1}^{N_t} e_i x_i^\top.$$

Let  $c = -2\eta$  and define  $G_i = e_i x_i^\top$ . Then

$$\Delta W_t = c \sum_{i=1}^{N_t} G_i. \tag{25}$$

**Empirical Support for Assumptions (A3) and (A4).** Across all architectures we evaluate (RoBERTa, GPT-2, ViT), the fine-tuning displacements  $\Delta W_t$  exhibit a striking empirical regularity: their entries are extremely close to zero-mean and follow a tightly concentrated Gaussian distribution. Figure 3 illustrates representative layers across the three model families, each showing near-perfect symmetry and Gaussian shape.

Under the linearized model  $\Delta W_t = c \sum_{i=1}^{N_t} G_i$  with  $G_i = e_i x_i^\top$ , the sample mean satisfies

$$\mathbb{E}[\Delta W_t] = c N_t \mathbb{E}[G].$$

The empirical observation that  $\Delta W_t$  is zero-mean therefore implies  $\mathbb{E}[G] \approx 0$ , and consequently

$$\mathbb{E}[e x^\top] \approx 0,$$

which is precisely the statement of Assumption (A3). Thus, (A3) is not an idealized mathematical simplification but a compact representation of the experimentally observed behavior of the fine-tuning updates.

A second empirical observation is that the covariance structure of  $\Delta W_t$  aligns spectrally with the input covariance  $\Sigma_t = \mathbb{E}[xx^\top]$ . Combining this with the identity

$$G^\top G = (e^\top e) xx^\top,$$

the simplest statistically consistent parametrization is

$$\mathbb{E}[G^\top G] = \mathbb{E}[(e^\top e) xx^\top] \approx \mathbb{E}[e^\top e] \mathbb{E}[xx^\top] = \sigma_{e,\text{total}}^2 \Sigma_t,$$

exactly matching Assumption (A4). In this sense, (A4) can be interpreted as formalizing the experimental observation that the variability of the update directions is proportional to the input covariance structure, where the constant of proportionality is a scalar residual-energy factor.

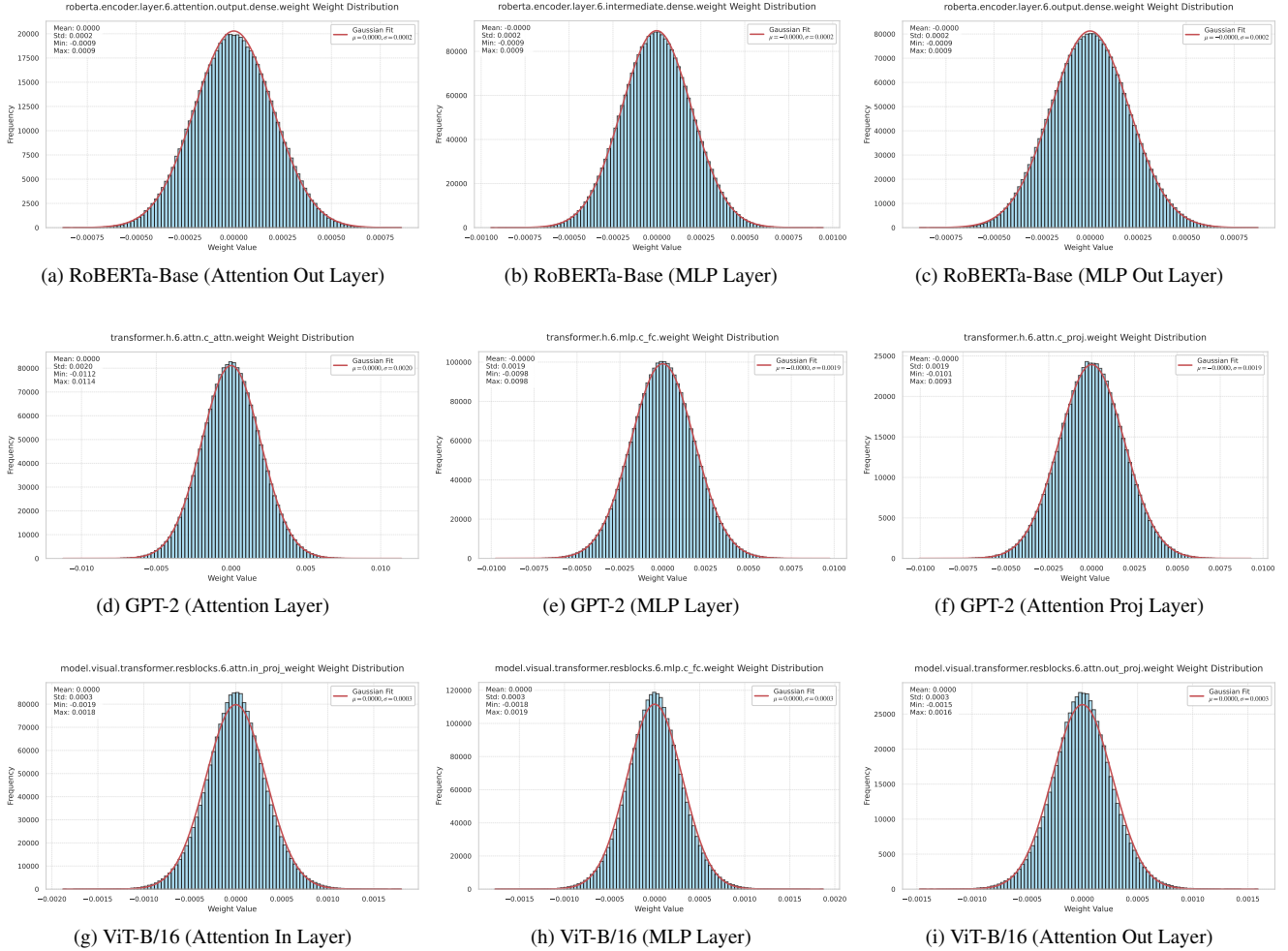


Figure 3. **Empirical distributions of  $\Delta W_t$  across architectures, layer types, and tasks.** Each subplot shows the histogram of the entries of  $\Delta W_t$  for one representative layer from RoBERTa-Base, GPT-2, and ViT-B/16. All distributions exhibit near-zero means and closely resemble Gaussian profiles, providing strong empirical support for our theoretical assumptions (A3) and (A4).

**Step 2: Covariance of  $\Delta W_t$ .** We define the covariance of the random matrix  $\Delta W_t$  in the Frobenius sense as

$$\text{Cov}(\Delta W_t) = \mathbb{E}[(\Delta W_t - \mathbb{E}[\Delta W_t])^\top (\Delta W_t - \mathbb{E}[\Delta W_t])]. \quad (26)$$

Our goal is to express this covariance in terms of the single-sample update matrices  $G_i$ .

Using the representation

$$\Delta W_t = c \sum_{i=1}^{N_t} G_i \quad \text{from (25),}$$

and applying the standard identity that the covariance of a sum of independent random variables (here applied to  $\text{vec}(\Delta W_t)$ ) is the sum of their individual covariances, we obtain

$$\text{Cov}(\Delta W_t) = c^2 \sum_{i=1}^{N_t} \text{Cov}(G_i) = c^2 N_t \text{Cov}(G), \quad (27)$$

where  $G$  is a generic copy of  $G_i$ . The covariance of the single-sample update matrix  $G$  is

$$\text{Cov}(G) = \mathbb{E}[G^\top G] - \mathbb{E}[G]^\top \mathbb{E}[G]. \quad (28)$$

Under Assumption (A3),

$$\mathbb{E}[G] = \mathbb{E}[ex^\top] = 0,$$

so the covariance simplifies to

$$\text{Cov}(G) = \mathbb{E}[G^\top G]. \quad (29)$$

Substituting this back yields the compact expression

$$\text{Cov}(\Delta W_t) = c^2 N_t \mathbb{E}[G^\top G]. \quad (30)$$

**Step 3: Single-sample second-order structure.** Recall that each update matrix is of the form  $G = ex^\top$  with  $e = W_0 x - y$ . A direct computation shows that

$$G^\top G = (ex^\top)^\top (ex^\top) = xe^\top e x^\top = (e^\top e) xx^\top.$$

Taking expectations and applying Assumption (A4),

$$\begin{aligned} \mathbb{E}[G^\top G] &= \mathbb{E}[(e^\top e) xx^\top] \\ &= \mathbb{E}[e^\top e] \mathbb{E}[xx^\top] \\ &= \sigma_{e,\text{total}}^2 \Sigma_t. \end{aligned} \quad (31)$$

Substituting (31) into (30), we obtain

$$\begin{aligned} \text{Cov}(\Delta W_t) &= c^2 N_t \mathbb{E}[G^\top G] \\ &= c^2 N_t \sigma_{e,\text{total}}^2 \Sigma_t. \end{aligned} \quad (32)$$

Since  $c^2 N_t \sigma_{e,\text{total}}^2$  is a scalar depending only on the learning rate and the aggregate residual energy, we conclude that

$$\text{Cov}_{\mathcal{D}_t}[\Delta W_t] \propto \Sigma_t. \quad (33)$$

This completes the proof under Assumptions (A1)–(A4).  $\square$

**Step 4: Discussion on the Role of the Mean Update.** The population expression for the covariance of the displacement can be written in the more general form

$$\text{Cov}(\Delta W_t) = c^2 N_t \left( \mathbb{E}[G^\top G] - \mathbb{E}[G]^\top \mathbb{E}[G] \right), \quad (34)$$

where the second term  $\mathbb{E}[G]^\top \mathbb{E}[G]$  captures the squared mean update and represents systematic (rather than stochastic) drift during fine-tuning.

In practice, we consistently observe that the empirical displacement  $\Delta W_t$  is extremely close to zero-mean (Fig. 3), implying that  $\mathbb{E}[G] = \mathbb{E}[ex^\top]$  is negligible. This is expected: modern pretrained models already provide strong representations

for downstream tasks, so the fine-tuning trajectory consists predominantly of small zero-mean fluctuations rather than large consistent shifts. Consequently,

$$\mathbb{E}[G]^\top \mathbb{E}[G] \ll \mathbb{E}[G^\top G],$$

and the contribution of the mean update term can be ignored at leading order.

Under this empirically justified simplification, Eq. (34) reduces to

$$\text{Cov}(\Delta W_t) \approx c^2 N_t \mathbb{E}[G^\top G],$$

which, by Step 3, yields

$$\text{Cov}(\Delta W_t) \approx (c^2 N_t \sigma_{e,\text{total}}^2) \Sigma_t.$$

Hence, the covariance of the weight displacement is governed primarily by the input covariance structure, even without strictly imposing Assumption (A3). This completes the argument that

$$\text{Cov}_{\mathcal{D}_t}[\Delta W_t] \propto \Sigma_t.$$

□

**Remark on Practical Estimation.** The proportionality  $\text{Cov}(\Delta W_t) \propto \Sigma_t$  is a population-level relation, where the expectation is taken over the stochasticity of fine-tuning (data sampling, minibatch order, and initialization noise). In practice, however, we only observe a single realization of  $\Delta W_t$  per task. As a result, the estimator used in the main paper does not attempt to reconstruct the full population covariance; instead, it extracts a second-order proxy from the observed weights:

$$\widehat{\Sigma}_t \propto (\Delta W_t - \mathbf{1}\mu_t^\top)^\top (\Delta W_t - \mathbf{1}\mu_t^\top),$$

where  $\mu_t$  is the column-wise mean and  $(\mathbf{1}\mu_t^\top)$  is a practical debiasing step.

Importantly, both the centered and uncentered quadratic forms differ only by a rank-one correction and share the same eigenvectors. Since `ACE-Merging` relies only on the spectral structure of  $\widehat{\Sigma}_t$ , the empirical estimator provides a faithful proxy whose principal directions are aligned with those of  $\Sigma_t$ , up to a global scaling factor. Since the empirical second-order profile extracted from  $\Delta W_t$  suffices for our closed-form merging procedure, exact covariance recovery is unnecessary.

#### A.4. Additional statistics for adaptive covariance normalization

In practice, we compute the Frobenius norm via its trace identity,  $\|\Delta W_t\|_F^2 = \text{Tr}(\Delta W_t^\top \Delta W_t)$ . Thus the heterogeneity coefficient introduced in Sec. 4.2 is implemented equivalently as:

$$\gamma = \frac{\text{Var}_t[\log \text{Tr}(\Delta W_t^\top \Delta W_t)]}{(\mathbb{E}_t[\log \text{Tr}(\Delta W_t^\top \Delta W_t)])^2}. \quad (35)$$

Since  $\|\Delta W_t\|_F^2 \equiv \text{Tr}(\Delta W_t^\top \Delta W_t)$ , Eq. (35) is mathematically identical to the original definition, and aligns exactly with our implementation.

As a lightweight measure for detecting the degree of mismatch among task-specific covariance matrices  $\{C_t\}$ . We reported results for RoBERTa-Base (8 tasks) and ViT-B/16 (14 tasks), where  $\gamma$  reliably separates homogeneous from heterogeneous task sets.

To provide more comprehensive evidence for the behavior of  $\gamma$  across architectures and numbers of tasks, we present additional statistics below.

**RoBERTa-Large on 8 tasks.** Fig. 4 shows the distribution of  $\{\tau_t\}$  and the resulting  $\gamma$  for RoBERTa-Large across the same 8 GLUE-style tasks used in the main paper. Similar to RoBERTa-Base, the heterogeneity score is high ( $\gamma > 0.3$ ), confirming a significant degree of task specificity.

**GPT-2 on 7 tasks.** Fig. 5 reports the corresponding values for GPT-2, where we observe noticeably larger spread in  $\{\tau_t\}$  and a higher  $\gamma$  compared to RoBERTa. This aligns with the empirical difficulty of merging GPT-2 task vectors (Sec. 5), as greater heterogeneity destabilizes simple isotropic corrections and motivates adaptive normalization.

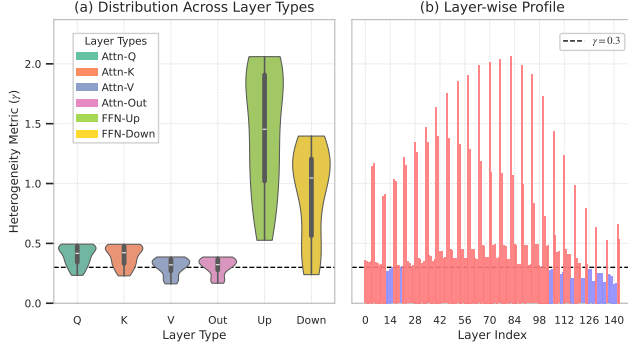


Figure 4. **RoBERTa-Large (8 tasks)**. Trace statistics  $\{\tau_t\}$  and heterogeneity coefficient  $\gamma$ .

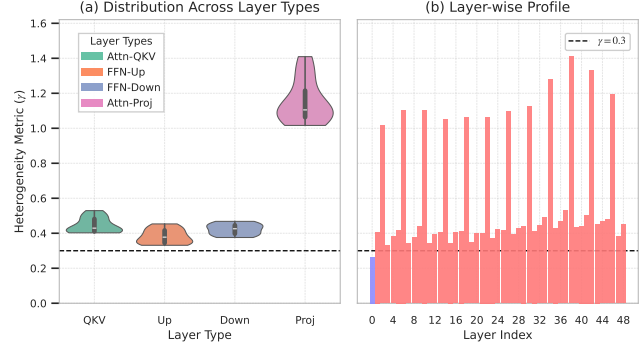


Figure 5. **GPT-2 (7 tasks)**. Larger heterogeneity  $\gamma$  compared to RoBERTa, indicating stronger mismatch among task covariances.

**Effect of increasing number of tasks (ViT-L/14).** To examine how heterogeneity evolves as more tasks are included, we evaluate  $\gamma$  for ViT-L/14 under multiple task-set sizes. In Fig. 6 and Fig. 7, we show the results for 8 and 20 tasks, representing the low- and high-diversity extremes. The heterogeneity coefficient increases noticeably when moving from 8 to 20 tasks, consistent with the overall monotonic trend observed across all task counts. This behavior supports our claim that task diversity naturally grows as more datasets are merged, reinforcing the need for the adaptive scaling mechanism introduced in Sec. 4.2.

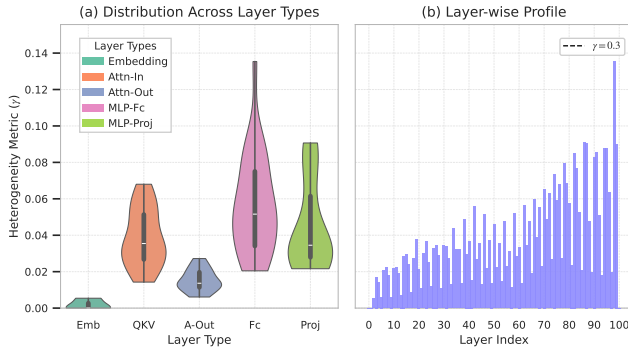


Figure 6. **ViT-L/14 (8 tasks)**. Moderate heterogeneity  $\gamma$ , indicating manageable variation across task covariances at smaller task scales.

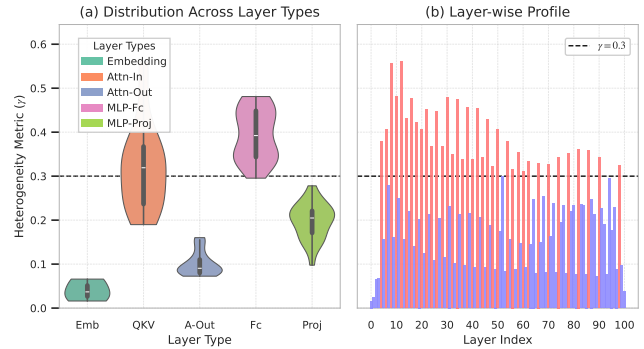


Figure 7. **ViT-L/14 (20 tasks)**. Substantially larger heterogeneity  $\gamma$ , showing increasing mismatch among task covariances as the number of merged tasks grows.

**Summary.** Across all architectures,  $\gamma$  reliably captures the heterogeneity of the task set:

- small  $\gamma$  indicates well-aligned task covariances, allowing simple merging procedures;
- large  $\gamma$  reveals strong variability, requiring the adaptive covariance normalization of ACE-Merging.

These results reinforce the robustness of  $\gamma$  as a criterion for activating heterogeneity-aware strategies.

## B. Computational Complexity of ACE-Merging and Baselines

We briefly compare the computational complexity of ACE-Merging with two representative baselines: the SVD-based TSV-M method [19] and the gradient-based WUDI-merging approach [23]. We use the following notation: let  $T$  be the number of task vectors and  $L$  be the number of merged layers. Let each linear layer weight matrix  $\Delta W_t$  have the shape  $d_{\text{out}} \times d_{\text{in}}$ . For simplicity in big- $O$  notation, we let  $n = \max(d_{\text{out}}, d_{\text{in}})$  and report per-layer complexities in terms of  $n$ .

**TSV-M.** TSV-M performs multiple singular value decompositions per layer, the complexity per layer is calculated by:

- $T$  SVDs on the  $(d_{\text{out}} \times d_{\text{in}})$  task matrices, costing  $O(T \cdot \min(d_{\text{out}}^2 d_{\text{in}}, d_{\text{out}} d_{\text{in}}^2)) = O(Tn^3)$ .
- Two additional SVDs on aggregated matrices, adding a lower-order cost of  $O(n^3)$ .

The total complexity per layer is therefore  $O(Tn^3)$ . Across all  $L$  layers, the overall complexity of TSV-M is

$$O(\text{TSV-M}) = O(L \cdot Tn^3) = O(LTn^3). \quad (36)$$

**Gradient-based merging (WUDI-merging).** In contrast, WUDI-merging optimizes the merged weights by iterative gradient descent. Let  $K$  denote the number of optimization steps. Each step requires evaluating the loss and its gradient by aggregating information across all  $T$  task vectors. The dominant computation in each forward-backward pass involves element-wise operations on tensors of size  $(T \times d_{\text{out}} \times d_{\text{in}})$ , costing  $O(Td_{\text{out}}d_{\text{in}}) = O(Tn^2)$  per layer. The total complexity is thus multiplicative in  $K$ ,  $L$ , and  $T$ :

$$O(\text{WUDI}) = O(K \cdot L \cdot T \cdot n^2) = O(KLTn^2). \quad (37)$$

In practice,  $K$  must be sufficiently large for convergence (e.g., hundreds of steps), making this approach computationally intensive compared to closed-form alternatives, especially for large models where  $n$  is substantial.

**ACE-Merging.** ACE-Merging avoids iterative optimization and computes the solution in closed form. Its complexity can be analyzed by its main computational steps on a per-layer basis:

- **Covariance Aggregation.** The algorithm iterates through all  $T$  task vectors to compute aggregated matrices. For each task, the dominant step is the matrix multiplication  $\Delta W_t^\top \Delta W_t$  to form the covariance proxy. This operation has a cost of  $O(d_{\text{out}} d_{\text{in}}^2)$ . The loop over  $T$  tasks makes this stage's complexity  $O(Td_{\text{out}} d_{\text{in}}^2)$ .
- **Closed-form Solution.** After the loop, the algorithm solves for the merged weights. This is dominated by a single inversion of a  $(d_{\text{in}} \times d_{\text{in}})$  matrix, which costs  $O(d_{\text{in}}^3)$ .
- **Spectral Refinement (Optional).** If applied, this step performs a single SVD on a  $(d_{\text{out}} \times d_{\text{in}})$  matrix, adding a cost of  $O(\min(d_{\text{out}}^2 d_{\text{in}}, d_{\text{out}} d_{\text{in}}^2))$ .

Summing these costs and using  $n = \max(d_{\text{out}}, d_{\text{in}})$ , the per-layer complexity is dominated by the aggregation step, resulting in  $O(Tn^3)$ . The total complexity over all  $L$  layers is therefore:

$$O(\text{ACE-Merging}) = O(L \cdot Tn^3) = O(LTn^3). \quad (38)$$

In summary, ACE-Merging matches the asymptotic complexity of SVD-based methods like TSV-M while being a closed-form solution. It offers a significant theoretical efficiency advantage over iterative methods like WUDI-merging, whose complexity scales with the number of optimization steps  $K$ , making them potentially less practical for large-scale problems.

## B.1. Analysis of Limiting Cases and Hyperparameters

We analyze how ACE-Merging behaves under limiting values of its key hyperparameters. These limits reveal how the method interpolates between simple averaging, weighted averaging, and full spectral refinement.

**Limit  $\epsilon \rightarrow \infty$  (strong Tikhonov regularization).** The hyperparameter  $\text{eps}(\epsilon)$  controls the amount of Tikhonov regularization added to each covariance proxy:

$$\Sigma_t \leftarrow \Sigma_t + \epsilon_t I.$$

As  $\epsilon \rightarrow \infty$ , the regularizer dominates the raw covariance estimates. Two regimes arise depending on whether heterogeneity is detected.

- **Low heterogeneity ( $\gamma \leq \gamma_{\text{thresh}}$ ).** In this mode, each task uses the same  $\epsilon_t = \epsilon$ , giving  $\Sigma_t \approx \epsilon I$ . Therefore

$$W_0 = \left( \sum_{t=1}^T W_t \Sigma_t \right) \left( \sum_{t=1}^T \Sigma_t \right)^{-1} \xrightarrow{\epsilon \rightarrow \infty} \frac{1}{T} \sum_{t=1}^T W_t.$$

Thus, ACE-Merging reduces to **simple averaging** (task arithmetic) when the covariances are made infinitely isotropic.

- **High heterogeneity ( $\gamma > \gamma_{\text{thresh}}$ ).** In this mode,  $\epsilon_t = \epsilon / \text{tr}(W_t^\top W_t)$ , giving  $\Sigma_t \approx (\epsilon / \tau_t) I$  with  $\tau_t = \text{tr}(W_t^\top W_t)$ . Then

$$W_0 \xrightarrow{\epsilon \rightarrow \infty} \frac{\sum_{t=1}^T \frac{1}{\tau_t} W_t}{\sum_{t=1}^T \frac{1}{\tau_t}},$$

i.e. a **weighted average** where tasks with larger Frobenius norms receive smaller weights.

Table 7. ACE-Merging accuracy (%) on ViT-B/32, ViT-B/16, and ViT-L/14 across increasing numbers of tasks.

Dataset	ViT-B/32			ViT-B/16			ViT-L/14		
	8	14	20	8	14	20	8	14	20
MNIST	99.46	99.22	92.65	99.44	99.32	96.40	99.58	99.59	96.65
Cars	71.67	68.59	61.90	81.54	78.24	72.40	90.34	88.46	85.37
DTD	89.63	82.45	75.80	90.69	83.19	76.33	96.97	93.19	88.67
EuroSAT	95.81	88.37	83.70	97.78	96.96	94.56	99.52	99.30	98.22
GTSRB	92.44	85.49	76.43	92.94	88.20	80.74	97.34	97.42	93.49
RESISC45	86.79	81.51	77.92	90.73	88.75	85.97	94.76	93.25	92.11
SUN397	73.06	70.75	68.63	76.57	74.04	72.07	81.83	78.62	76.72
SVHN	94.19	90.10	82.89	95.08	93.22	88.40	96.20	95.61	91.80
PCAM	—	84.09	83.75	—	86.14	85.02	—	85.82	85.77
CIFAR100	—	72.77	68.79	—	78.41	75.64	—	86.64	83.75
STL10	—	97.50	96.73	—	98.15	97.58	—	99.41	99.34
Oxford-IIIT Pet	—	90.54	88.20	—	93.98	92.86	—	96.43	96.18
Flowers102	—	73.04	70.19	—	79.07	76.24	—	87.32	84.57
FER2013	—	67.62	63.46	—	68.04	63.81	—	73.92	69.95
CIFAR10	—	—	93.54	—	—	95.55	—	—	98.05
Food101	—	—	80.71	—	—	88.47	—	—	93.98
RenderedSST2	—	—	72.43	—	—	77.10	—	—	85.56
EMNIST	—	—	98.07	—	—	97.82	—	—	99.52
Fashion-MNIST	—	—	83.50	—	—	88.07	—	—	91.15
KMNIST	—	—	57.27	—	—	37.23	—	—	78.95
<b>Average</b>	87.88	82.29	78.83	90.60	86.12	82.11	94.57	91.07	89.49

**Role of the heterogeneity threshold  $\gamma_{\text{thresh}}$ .** This threshold determines whether trace normalization and spectral refinement are activated.

- If  $\gamma_{\text{thresh}}$  is very large, the condition  $\gamma > \gamma_{\text{thresh}}$  is almost never met, so ACE-Merging behaves like a regularized multi-task regression method without any task-specific normalization.
- If  $\gamma_{\text{thresh}} \rightarrow 0$ , the high-heterogeneity branch is always selected, enabling trace normalization and spectral refinement for all task sets.

**Role of the spectral fraction  $k_{\text{frac}}$ .** This hyperparameter determines the rank of the spectral refinement term added to the closed-form solution  $W_0$ . As implemented,

$$\Delta_{\text{spec}} = \sigma_{\text{iso}} U_k V_k^T, \quad \sigma_{\text{iso}} = \frac{1}{k} \sum_{i=1}^k S_i,$$

where  $S_i$  are the top singular values of the fused residual.

- As  $k_{\text{frac}} \rightarrow 0$ ,  $k \rightarrow 0$  and the refinement term vanishes, giving the pure closed-form solution  $W_0$ .
- As  $k_{\text{frac}} \rightarrow 1$ , the correction uses all singular vectors, producing a full-rank spectral adjustment whose singular values are replaced by their mean. This yields a *uniform spectral correction* added to  $W_0$ , rather than a full isotropization.

Thus,  $k_{\text{frac}}$  provides a continuous control over how much shared spectral structure is reintroduced after the adaptive merging step.

### C. ACE-Merging Performance on ViT Models with Increasing Task Coverage

We report the full performance of ACE-Merging on three vision transformer backbones: ViT-B/32, ViT-B/16, and ViT-L/14, evaluated under increasing numbers of downstream tasks. These results complement the heterogeneity analysis in Sec. 4.2 and empirically demonstrate that ACE-Merging remains stable as task diversity grows. All values are test classification accuracies unless otherwise specified.

Each table presents side-by-side results for 8, 14, and 20 tasks, and includes the average accuracy over all tasks for each backbone and setting.

Table 8. **LLaMA-3 merging results (raw scores)**. Single-task fine-tuning experts and merged models evaluated on five benchmarks.

Tasks	xquad_zh	xquad_vi	gsm8k_cot	mathqa	humaneval
multilingual	27.24	42.20	–	–	–
coding	–	–	–	34.30	49.39
math	–	–	74.00	–	–
Average	8.40	32.72	73.62	34.24	46.34
Task Arithmetic	8.06	32.88	73.09	34.14	46.34
ACE (ours)	16.42	37.68	69.75	34.57	50.61

Table 9. **Normalized performance on LLaMA-3 (%)**. Each value is the ratio between the merged model and the best single-task fine-tuning expert for that benchmark.

Method	xquad_zh	xquad_vi	gsm8k_cot	mathqa	humaneval	Avg.
Average	30.84	77.54	99.49	99.83	93.82	80.30
Task Arithmetic	29.59	77.91	98.77	99.53	93.82	79.92
ACE (ours)	60.28	89.29	94.26	100.79	102.47	89.42

### C.1. Additional results on LLaMA-3 and out-of-domain generalization

We further evaluate ACE-Merging on a LLaMA-3 backbone fine-tuned on three specialized expert task groups: multilingual QA (multilingual), code generation (coding), and mathematical reasoning (math). Each expert is fine-tuned on a disjoint subset of benchmarks and then merged using different weight-space fusion strategies. The merged models are evaluated jointly on five downstream benchmarks: xquad\_zh, xquad\_vi, gsm8k\_cot, mathqa, and humaneval. The raw scores are reported in Tab. 8.

To normalize for the different intrinsic difficulty and scale of each benchmark, we further report in Tab. 9 the performance of the merged models as a percentage of their corresponding single-task fine-tuning expert. For each column, we divide the merged score by the score of the relevant expert (multilingual for xquad\_zh and xquad\_vi, math for gsm8k\_cot, and coding for mathqa and humaneval) and multiply by 100.

The normalized results highlight the out-of-domain behavior of ACE-Merging. On the multilingual benchmarks xquad\_zh and xquad\_vi, which are out-of-domain for both the coding and math experts, ACE-Merging recovers 60.28% and 89.29% of the corresponding single-task fine-tuning performance, substantially outperforming both simple averaging and task arithmetic (which remain around 30–78%). On the code benchmark humaneval, ACE-Merging even slightly exceeds the coding expert, achieving 102.47% of the fine-tuned score, while maintaining competitive accuracy on gsm8k\_cot and mathqa. Overall, ACE-Merging attains the highest normalized average score (89.42%), indicating that it effectively aggregates heterogeneous experts and exhibits strong out-of-domain generalization across multilingual, coding, and mathematical reasoning tasks.